

# The effect of magnetic dipolar interactions on the interchain spin wave dispersion in $\text{CsNiF}_3$

M. Baehr, M. Winkelmann, P. Vorderwisch, M. Steiner

\*C. Pich, \*F. Schwabl

*BENSC, Hahn-Meitner-Institut, Glienickerstr. 100, 14109 Berlin, Germany*

*\*TU-München, James-Frank-Strasse, 85747 Garching, Germany*

Inelastic neutron scattering measurements were performed on the ferromagnetic chain system  $\text{CsNiF}_3$  in the collinear antiferromagnetic ordered state below  $T_N = 2.67$  K. The measured spin wave dispersion was found to be in good agreement with linear spin wave theory including dipolar interactions. The additional dipole tensor in the Hamiltonian was essential to explain some striking phenomena in the measured spin wave spectrum: a peculiar feature of the dispersion relation is a jump at the zone center, caused by strong dipolar interactions in this system. The interchain exchange coupling constant and the planar anisotropy energy were determined within the present model to be  $J'/k_B = -0.0247(12)$  K and  $A/k_B = 3.3(1)$  K. This gives a ratio  $J/J' \approx 500$ , using the previously determined intrachain coupling constant  $J/k_B = 11.8$  K. The small exchange energy  $J'$  is of the same order as the dipolar energy, which implies a strong competition between the both interactions.

PACS numbers: 75.10 J, 75.30 D, 75.30 G, 75.50 E

## I. INTRODUCTION

The compound  $\text{CsNiF}_3$  is the best known example of a quasi one-dimensional (1D) ferromagnet. It crystallizes in the hexagonal  $\text{ABX}_3$  type structure ( $\text{P6}_3/\text{mmc}$ , with  $a = b = 6.21\text{\AA}$  and  $c = 5.2\text{\AA}$ ) [1]. The  $\text{Ni}^{2+}$  ions ( $S=1$ ) are located in the centers of  $\text{NiF}_6$ -octahedra, which are linked by common faces to form chains along the  $c$  axis. A series of fundamental investigations on linear and non-linear spin dynamics above  $T_N$  [6] and in an external magnetic field have been performed [2,3]. Below  $T_N = 2.67$  K three-dimensional ordering sets in due to an isotropic interchain interaction and the dipolar interaction. The Hamiltonian describing the three-dimensional magnetic properties of  $\text{CsNiF}_3$  is

$$H = -2J \sum_i \mathbf{S}_i \mathbf{S}_{i+1} + A \sum_l (S_l^z)^2 - \sum_{l,l'} \left( J'_{ll'} \delta^{\alpha\beta} + A_{ll'}^{\alpha\beta} \right) S_l^\alpha S_{l'}^\beta. \quad (1)$$

The index  $i$  indicates positions on single spin chains, whereas  $l$  indicates all spin positions. In Eq. (1) the first two terms are responsible for the one-dimensional behavior, i.e.  $J$  denotes the ferromagnetic intrachain interaction and  $A$  the single-ion anisotropy. The last two terms lead to the three-dimensional order, where  $J'_{ll'}$  denotes the nearest neighbor interchain interaction and  $A_{ll'}^{\alpha\beta}$  the long-range dipolar interaction

$$A_{l,l'}^{\alpha\beta} = -\frac{(g\mu_B)^2}{2} \left\{ \frac{\delta^{\alpha\beta}}{|\mathbf{x}_l - \mathbf{x}_{l'}|^3} + \frac{3(\mathbf{x}_l - \mathbf{x}_{l'})^\alpha (\mathbf{x}_l - \mathbf{x}_{l'})^\beta}{|\mathbf{x}_l - \mathbf{x}_{l'}|^5} \right\} \quad (2)$$

The coupling constant along the chain  $J$  and the anisotropy energy  $A$  were determined by inelastic neutron scattering in the one dimensional ordered state ( $T > T_N$ ) to be  $J/k_B = 11.8$  K and  $A/k_B = 4.5$  K [2]. These values are based on linear spin wave theory for classical spins [4], whereas a larger anisotropy constant  $A = 9.0K$  was determined, using a renormalized spin wave theory for  $S = 1$  spins [5] considering the continuous degeneracy of the ground state. In both analyses the third and fourth term of Eq. (1) had been neglected, which are important for the three-dimensional ordering of  $\text{CsNiF}_3$  especially the dipolar interaction as indicated by the antiferromagnetic, collinear ordered ground state [6].

In the three-dimensional state a purely isotropic antiferromagnetic exchange coupling leads to a frustrated  $120^\circ$  structure in hexagonal  $\text{ABX}_3$  compounds [8,9,10]. In the limit of

pure dipole interaction a ferromagnetic spin arrangement is favored as in the case of a pure two-dimensional triangular lattice [11,18]. However, if dipolar and exchange energies are of the same order a collinear antiferromagnetic structure occurs which will be shown later. Due to the collinear order of the spins, the ground state is no more continuously degenerate but shows three different domains (A,B,C), as shown in Fig. (1) [12,6].

While the spin dynamics above  $T_N$  are well known, the spin wave excitations in the ordered state ( $T < T_N$ ) have not yet been studied in detail. The aim of the present investigation is to determine the interchain coupling constant and to probe the effects of the dipolar interaction on the spin wave spectrum. The evaluation of the interchain magnon dispersion relation and the related neutron scattering cross sections were performed, using quantum mechanical spin wave theory including long-range dipolar interactions.

## II. THEORY

In this chapter we derive the excitation spectrum and the scattering amplitudes within the linear spin-wave theory for the Heisenberg Hamiltonian in Eq. (1).

### A. Excitation spectrum

In this section the dispersion relation for domain A will be derived. In the following we choose the Cartesian coordinate system shown in Fig. (1) and the Brillouin zone as in Fig. (2). Fourier transform of the Hamiltonian (Eq. (1)) yields

$$H = - \sum_{\mathbf{q}} \left( J_{\mathbf{q}} \delta^{\alpha\beta} - A \delta^{\alpha z} \delta^{\beta z} + J'_{\mathbf{q}} \delta^{\alpha\beta} + A_{\mathbf{q}}^{\alpha\beta} \right) S_{\mathbf{q}}^{\alpha} S_{-\mathbf{q}}^{\beta} , \quad (3)$$

with the nearest-neighbor exchange energies (intrachain and interchain)

$$J_{\mathbf{q}} = 2J \cos q_z \quad (4)$$

$$J'_{\mathbf{q}} = 2J' \left( \cos q_x + 2 \cos \frac{q_x}{2} \cos \frac{\sqrt{3}q_y}{2} \right) . \quad (5)$$

The Fourier transform of the dipole tensor  $A_{\mathbf{q}}^{\alpha\beta}$ , is obtained via Ewald summation technique [13]. The Holstein-Primakoff transformation, which introduces Bose operators  $a_l$  and  $a_l^\dagger$ , is given up to bilinear order [14] by

$$S_l^x = \pm(S - a_l^\dagger a_l), \quad (6a)$$

$$S_l^y = \sqrt{\frac{S}{2}}(a_l + a_l^\dagger), \quad (6b)$$

$$S_l^z = \mp i\sqrt{\frac{S}{2}}(a_l - a_l^\dagger), \quad (6c)$$

where the upper (lower) sign corresponds to the first (second) sublattice. After Fourier transformation of these equations and insertion into the Hamiltonian (Eq. (3)), regarding only wave vectors perpendicular to the chain axis ( $q_z = 0$ ), the bilinear term becomes

$$H^{(2)} = \sum_{\mathbf{q}} A_{\mathbf{q}} a_{\mathbf{q}}^\dagger a_{\mathbf{q}} + \frac{1}{2} B_{\mathbf{q}} (a_{\mathbf{q}} a_{-\mathbf{q}} + a_{\mathbf{q}}^\dagger a_{-\mathbf{q}}^\dagger), \quad (7)$$

with the coefficients

$$A_{\mathbf{q}} = SA + S(2J'_{\mathbf{q}_1} - J'_{\mathbf{q}} - J'_{\mathbf{q}+\mathbf{q}_1}) + S(2A_{\mathbf{q}_1}^{xx} - A_{\mathbf{q}}^{yy} - A_{\mathbf{q}+\mathbf{q}_1}^{zz}) \quad (8)$$

$$B_{\mathbf{q}} = -SA + S(J'_{\mathbf{q}+\mathbf{q}_1} - J'_{\mathbf{q}}) + S(A_{\mathbf{q}+\mathbf{q}_1}^{zz} - A_{\mathbf{q}}^{yy}). \quad (9)$$

Due to the large planar anisotropy  $A$ , for the experiments explained below, it is sufficient to study only fluctuations within the hexagonal plane. The full expression for arbitrary wave vectors will be given in [18]. The wave vector  $\mathbf{q}_1 = 2\pi/\sqrt{3}(0, 1, 0)$  (corresponding to  $(\frac{1}{2}, 0, 0)$  in reciprocal lattice units (r. l. u.)) describes the antiferromagnetic modulation of the ground state. After diagonalizing this Hamiltonian via a Bogoliubov transformation we obtain the dispersion relation

$$\begin{aligned} E_{\mathbf{q}} &= \sqrt{A_{\mathbf{q}}^2 - B_{\mathbf{q}}^2} \\ &= 2S\sqrt{(J'_{\mathbf{q}_1} - J'_{\mathbf{q}} + A_{\mathbf{q}_1}^{xx} - A_{\mathbf{q}}^{yy})(A + J'_{\mathbf{q}_1} - J'_{\mathbf{q}+\mathbf{q}_1} + A_{\mathbf{q}_1}^{xx} - A_{\mathbf{q}+\mathbf{q}_1}^{zz})}. \end{aligned} \quad (10)$$

Equation (10) holds for the crystallographic Brillouin zone (hexagon). In the smaller magnetic Brillouin zone (rectangular, see Fig. (2)) there are two modes which have the form

$$E_{\mathbf{q}}^{(1)} = \sqrt{A_{\mathbf{q}}^2 - B_{\mathbf{q}}^2} \quad (11a)$$

$$E_{\mathbf{q}}^{(2)} = \sqrt{A_{\mathbf{q}+\mathbf{q}_1}^2 - B_{\mathbf{q}+\mathbf{q}_1}^2} . \quad (11b)$$

Stability of the ground state requires that, for all wave vectors in the Brillouin zone,  $A_{\mathbf{q}} > |B_{\mathbf{q}}|$ , i.e.

$$J'_{\mathbf{q}_1} - J'_{\mathbf{q}} > A_{\mathbf{q}_1}^{xx} - A_{\mathbf{q}}^{yy} . \quad (12)$$

This condition gives an upper boundary for the exchange energy for  $\mathbf{q} = 0$  and a lower bound for  $\mathbf{q} = \mathbf{q}_0 = 4\pi/3(1, 0, 0)$  (or  $\mathbf{q} = (-\frac{1}{3}, \frac{2}{3}, 0)$  in r.l.u.)

$$A_{\mathbf{q}_1}^{xx} - A_{\mathbf{q}_0}^{xx} < J' < (A_{\mathbf{q}_1}^{xx} - A_0^{yy})/8 . \quad (13)$$

Note that the allowed range for the exchange energy depends (due to the restriction to  $q_z = 0$ ) explicitly neither on the ferromagnetic exchange  $J$  nor on the anisotropy energy  $A$ . Using the in-plane lattice constant  $a = 6.21\text{\AA}$  and the experimentally determined Landé factor  $g = 2.25$  [3] of  $\text{CsNiF}_3$ , the stability range for the exchange energy can be calculated to be [17]

$$-92\text{mK} < \frac{J'}{k_B} < -3\text{mK} . \quad (14)$$

## B. Scattering amplitudes

The inelastic magnetic scattering cross section is proportional to [15]

$$\frac{\partial^2 \sigma}{\partial \Omega \partial \omega} \propto \sum_{\alpha\beta} |F(\mathbf{Q})|^2 \left( \delta^{\alpha\beta} - \frac{Q_\alpha Q_\beta}{Q^2} \right) \int_{-\infty}^{\infty} \frac{dt}{2\pi} e^{-i\omega t} \langle S_{\mathbf{q}}^\alpha(t) S_{-\mathbf{q}}^\beta \rangle . \quad (15)$$

Here  $\mathbf{Q}$  denotes momentum transfer (scattering vector),  $F(\mathbf{Q})$  is the magnetic form factor and  $\mathbf{q}$  the wave vector to the nearest reciprocal lattice vector or position in the Brillouin zone  $\tau$  ( $\mathbf{Q} = \tau + \mathbf{q}$ ). In linear spin wave theory the spin-spin correlation functions can be evaluated with the Fourier transformed Eqs. (6a,6b,6c) and the Bogoliubov transformation. The cross section takes the form:

$$\frac{\partial^2 \sigma}{\partial \Omega \partial \omega} \propto |F(\mathbf{Q})|^2 \left[ \left( 1 - \frac{Q_y^2}{Q^2} \right) \frac{(A_{\mathbf{q}} - B_{\mathbf{q}})}{E_{\mathbf{q}}^{(1)}} \left\{ (1 + n_{\mathbf{q}}) \delta(\omega - E_{\mathbf{q}}^{(1)}) + n_{\mathbf{q}} \delta(\omega + E_{\mathbf{q}}^{(1)}) \right\} + \right. \\ \left. \left( 1 - \frac{Q_z^2}{Q^2} \right) \frac{(A_{\mathbf{q}+\mathbf{q}_1} + B_{\mathbf{q}+\mathbf{q}_1})}{E_{\mathbf{q}}^{(2)}} \left\{ (1 + n_{\mathbf{q}}) \delta(\omega - E_{\mathbf{q}}^{(2)}) + n_{\mathbf{q}} \delta(\omega + E_{\mathbf{q}}^{(2)}) \right\} \right]. \quad (16)$$

For neutrons, only spin fluctuations perpendicular to the momentum transfer  $\mathbf{Q}$  are detectable, meaning modes with magnetization vector parallel to the momentum transfer are invisible. Note that the first mode  $E_{\mathbf{q}}^{(1)}$  is only observable through the in-plane fluctuations  $\langle S^y S^y \rangle$  and the second mode  $E_{\mathbf{q}}^{(2)}$  through the out-of-plane fluctuations  $\langle S^z S^z \rangle$ . Thus, the first mode ( $E_{\mathbf{q}}^{(1)}$ ) will be called in-plane mode and the second mode ( $E_{\mathbf{q}}^{(2)}$ ) out-of-plane mode. Due to the strong planar anisotropy ( $A$ ) the in-plane fluctuations are more pronounced than the out-of-plane fluctuations, which can be seen by inserting Eqs. (8) and (9) for  $A_{\mathbf{q}}$  and  $B_{\mathbf{q}}$ . The ratio of the two prefactors is given by

$$\frac{A_{\mathbf{q}} - B_{\mathbf{q}}}{A_{\mathbf{q}+\mathbf{q}_1} + B_{\mathbf{q}+\mathbf{q}_1}} = \frac{A + J'_{\mathbf{q}_1} - J_{\mathbf{q}+\mathbf{q}_1} + A_{\mathbf{q}_1}^{xx} - A_{\mathbf{q}+\mathbf{q}_1}^{yy}}{J'_{\mathbf{q}_1} - J_{\mathbf{q}+\mathbf{q}_1} + A_{\mathbf{q}_1}^{xx} - A_{\mathbf{q}+\mathbf{q}_1}^{zz}}. \quad (17)$$

This leads to a very small neutron scattering cross section of the out-of-plane mode.

### III. EXPERIMENT

The measurements were carried out using the cold source triple axis spectrometer V2 at BENSC (Hahn-Meitner-Institut). Pyrolytic graphite (PG) crystals were used as monochromator and analyzer. The higher-order wavelength contributions were suppressed by using a liquid-N<sub>2</sub> cooled Be-filter. The crystal had a volume of about 1.5 cm<sup>3</sup>, and was mounted with the  $(a^*, c^*)$  plane in the scattering plane. A series of constant-Q scans at positions  $(Q_a, 0, 0)$  and  $(Q_a, 0, 2)$  were performed at  $T = 1.5$  K. The final energy at the  $Q_c = 0$  positions ( $(Q_a, 0, 0)$  scans) was fixed to be  $E_f = 2.98$  meV (collimation: neutron guide (NG) -40'-40'-40'). The collimation of the neutron guide for the used values of  $k_i$  is approximately 60'. At the  $Q_c = 2$  positions ( $(Q_a, 0, 2)$  scans) the final energy was increased to  $E_f = 4.66$  meV (collimation: NG-20'-20'-20'). The capital letters  $Q_{a,b,c}$  denote absolute Q values, while

$q_{a,b,c}$  represents the relative distance to the center of the Brillouin zone. At all  $Q_c = 0$  positions only one excitation peak was observable. The data at  $\mathbf{Q} = (0.8, 0, 0)$  ( $\mathbf{q} = (0.2, 0, 0)$ ) is shown as a representative example in Fig. 3. The profile of the incoherent background (centered at  $E = 0$ ) and the excitation signal were fitted by Gauss-peaks. The line widths are consistent with the expected instrument resolution. As discussed in the previous section, the in-plane mode has a much larger scattering amplitude ( $\sim 6$  times) than the out-of-plane mode. Nevertheless, the in-plane mode from domain A cannot be detected, because  $\mathbf{Q}$  is parallel to  $\mathbf{y}$  (see fig. 1). Thus, only the in-plane modes from domains B and C should be visible.

This was probed by a separate measurement in a horizontal magnetic field. In zero field all three magnetic domains of the crystal have approximately the same size. The relative volume parts of the different domains can be varied by applying an external magnetic field perpendicular to the  $c$ -axis [6]. A horizontal field parallel to  $a^*$  stabilizes domain A by the possibility of a slight spin canting. This is shown by the increasing intensity of the  $(0.5, 0, 0)$  Bragg reflection, when increasing the magnetic field (insert of Fig. 4). At a field of about 700 Gauss only domain A remains. Higher fields give rise to an increased spin canting, leading to a paramagnetic phase above 3000 Gauss. Figure 4 shows the spin wave excitation at  $\mathbf{Q} = (0.7, 0, 0)$  ( $\mathbf{q} = (0.3, 0, 0)$ ) for three different small magnetic fields. The narrow windows of the used cryomagnet limited the final energy to the value  $E_f = 4.06$  meV ( $k_f = 1.4 \text{ \AA}^{-1}$ ) (collimation: NG-40'-40'-40'). Thus, the resolution was lower in this experiment compared to the zero field measurements performed with  $E_f = 2.98$  meV ( $k_f = 1.2 \text{ \AA}^{-1}$ ). Obviously, the increase in the magnetic field reduces the intensity of the excitation, which confirms that the excitations at  $\mathbf{Q} = (Q_a, 0, 0)$  arise from the magnetic domains B and C.

For measuring the in-plane-mode in domain A, one has to use a momentum transfer  $\mathbf{Q}$  not parallel to the  $a^*$ -axis ( $y$ -direction). This was done by choosing  $\mathbf{Q} = (Q_a, 0, 2)$  (The size of the magnetic Brillouin zone in  $c^*$  direction is twice the size of the crystalline Brillouin zone). Unfortunately, the high  $Q$  values restricted  $E_f$  to large values ( $E_f = 4.66$  meV;  $k_f = 1.5 \text{ \AA}^{-1}$ ). This caused a coarse resolution compared to the measurement at  $\mathbf{Q} = (Q_a, 0, 0)$  even with

a better collimation (NG-20'20'20'). The measurement at  $\mathbf{Q} = (0.8, 0, 2)$  ( $\mathbf{q} = (0.2, 0, 0)$ ) is shown in (Fig. 5). At first glance, there seems to be just one excitation at about 0.15 meV. However, knowing the existence of an excitation at 0.118 meV from the measurement at  $\mathbf{Q} = (0.8, 0, 0)$  it is possible to fit a second excitation at 0.175(5) meV. The fit includes: two Gaussian peaks with fixed energy ( $\pm 0.118$  meV), one Gaussian peak for the incoherent background ( $E = 0$  meV) and one Gaussian peak for the second excitation. The widths of the different Gaussians were fitted independently. As for the measurements at  $(Q_a, 0, 0)$ , the line widths are caused by instrument resolution. All other measurements at  $(Q_a, 0, 2)$  were treated in the same way, except the measurement at  $(0.6, 0, 2)$  where the widths of all Gaussians were set equal.

#### IV. DISCUSSION AND CONCLUSION

The calculation of the dispersion relation was performed for the spin configuration of domain A. For comparison of the measured data with the theory, it is convenient to transform the signals from domains B and C to equivalent points in domain A. This can be done simply by rotations of the reciprocal lattice through  $\pm 60^\circ$ , which change the measured  $Q$  positions from  $(q_a, 0, 0)$  to  $(0, q_b, 0)$ . The data obtained from the measurements at  $(Q_a, 0, 2)$  belong already to domain A.

All measured data points of the dispersion relation are plotted in Fig. (6). The theoretical dispersion relation derived in section II (Eq. (10)) was fitted to these experimental data. The fit included just two free parameters: the value of the interchain exchange interaction  $J'$  and the easy-plane-anisotropy  $A$ . Good agreement between theory and experiment can be obtained with the values:

$$J'/k_B = -0.0247(12)K$$

$$A/k_B = 3.3(1)K.$$

The determined value of  $J'$  is consistent with the condition for the stability of the ground state (Eq. (14)). It turns out that  $\text{CsNiF}_3$  is far away from the transitions mentioned in



section I, and thus neglecting higher order terms in the Holstein-Primakoff transformation is expected to be a reliable low-temperature approximation. The value for the easy-plane anisotropy  $A$  of 3.3 K is lower than an earlier value ( $A_{1D}/k_B = 4.5$  K), determined from neutron scattering experiments using a linear spin wave theory above  $T_N$ . The actual difference is even larger, because the new value represents the pure crystal field anisotropy, while in the old measurements the effect of the intrachain dipolar interaction was not separated from the single site anisotropy.  $A_{1D}$  is an effective anisotropy. To compare these two values one has to calculate the dipolar anisotropy  $D$  in isolated spin chains, which leads to  $D \approx -0.64$  K. The calculation of  $D$  is possible by assuming a strictly ferromagnetic ordering of the spins along the magnetic chain. The good convergence of dipolar sums in one dimension, causes this value to be reached even for short-range ordered chains. The easy-axis-type dipolar anisotropy  $D$  has to be added to the easy-plane pure crystal field anisotropy  $A$  to give the old value of  $A_{1D} = D + A = 4.5$  K. Thus, the value for  $A$  from the measurements at  $T > T_N$  is  $A/k_B = 5.1$  K. A possible source of this difference is the neglect of the dipolar inter-chain interaction in the model used in the temperature range above  $T_N$ . Maybe, an independent determination of  $A$  by measuring the dispersion relation along the  $c$ -direction in the long-range ordered antiferromagnetic state ( $T < T_N$ ) is necessary to solve this problem.

The influence of each parameter of the Heisenberg-Hamiltonian (1) on the dispersion relation is directly visible at characteristic points of the Brillouin zone. Inserting Eq. (5) into Eq. (10) gives the following expressions for the excitation energies at the  $\mathbf{Q}$ -positions of  $\Gamma$ , P, X and S:

$$E_{\Gamma}^{(1)} = E_{\Gamma} = 2S\sqrt{(-8J' + A_P^{xx} - A_{\Gamma}^{yy})(A + A_P^{xx} - A_P^{zz})} \quad (18)$$

$$E_{\Gamma}^{(2)} = E_P = 2S\sqrt{(A_P^{xx} - A_P^{yy})(A - 8J' + A_P^{xx} - A_P^{zz})} \quad (19)$$

$$E_S = 2S\sqrt{(-4J' + A_P^{xx} - A_S^{yy})(A - 4J' + A_P^{xx} - A_S^{zz})} \quad (20)$$

$$E_X = 2S\sqrt{(A_P^{xx} - A_X^{yy})(A + A_P^{xx} - A_X^{zz})} \quad (21)$$

The values of the gap at the point  $\Gamma$  are determined by the single ion anisotropy and the

dipolar interaction. The in-plane mode  $E_{\Gamma}^{(1)}$  exhibits a gap even without dipolar terms, but the gap of the out-of-plane mode  $E_{\Gamma}^{(2)}$  vanishes in case of no dipolar interaction.

Two features of the dispersion relation are very unusual, and demonstrate the strong influence of the dipolar interaction in  $\text{CsNiF}_3$ : the position of the minimum of the dispersion relation and the jump of the dispersion relation at the Brillouin zone center. Contrary to common spin wave dispersion relations the energy minimum is not found at the magnetic zone center, but near the magnetic Brillouin zone boundary. This is due to the strong anisotropy of the dipolar interaction and the competition of the dipolar and exchange interaction.

The jump in the dispersion relation at the zone center  $\Gamma$  as shown in Fig. (6) can be viewed at in a similar way as the well known splitting of the longitudinal and transverse optical phonon modes in polar crystals. The LO–TO–splitting is caused by electric long-range dipolar interactions. This is used, for instance, for the derivation of the Lyddane–Sachs–Teller relation in solid state physics textbooks (e.g. [21]). The splitting is a result of the semi-convergence of dipole sums in homogeneously polarized systems. This gives rise to a depolarization field for longitudinal phonons with long wavelength, but not for transverse modes.

Similar arguments are valid for spin waves in  $\text{CsNiF}_3$ . Here, not only the large influence of the dipolar interaction is important, but also the planar anisotropy, leading to a linear polarized dynamic magnetization in the out-of-plane and in-plane modes. This allows to describe the in-plane mode in analogy to phonons as “longitudinal” or “transverse” spin wave, depending on the angle between dynamic magnetization ( $\mathbf{q}_a$ -direction) and propagation direction of the wave (Fig. 7). In common notation both are transverse spin fluctuations in respect to the spin orientation. As in the case of phonons, the “longitudinal” spin waves have the highest energy (wave propagation along  $\mathbf{q}_a$ ). In the observed plane of the  $Q$ -space ( $q_c = 0$ ) the out-of-plane mode is “transverse” for all spin wave propagation directions. Thus, the dispersion relation of this mode exhibits no jump at  $\Gamma$ .

In summary it is shown, that the description of the spin system of  $\text{CsNiF}_3$  including long-range dipolar interactions gives a convincing explanation for the unusual antiferromagnetic structure and spin dynamics. Especially, peculiar features of the spin wave dispersion relation can only be explained by a strong influence of long-range dipolar interactions in  $\text{CsNiF}_3$ . The jump of the spin wave dispersion relation at the zone center has been so far observed only in very few ferromagnets [22].  $\text{CsNiF}_3$  is the first antiferromagnet exhibiting this feature. This is caused by special properties of the one dimensional spin system  $\text{CsNiF}_3$ . Firstly, the strong 1D ferromagnetic order leads to a dipolar interchain interaction in the same order as the weak exchange interaction  $J'$ . Secondly, the planar anisotropy enforces a special spin dynamic, which gives rise to a dynamical magnetization pattern in long-wavelength spin waves. This demonstrated once again that low dimensional magnets are very suitable model systems to study a wide range of fundamental magnetic properties.

## ACKNOWLEDGMENTS

This work has been supported by the German Federal Ministry for Research and Technology (BMBF) under the contract number 03-SC4TUM

## REFERENCES

- [1] D. Babel, Z. anorg. allg. Chem. **369**, 117 (1969).
- [2] M. Steiner, J. Villain, and C.G. Windsor, Adv. Phys. **25**, 87 (1976).
- [3] M. Steiner and M. J. Mikeska, Adv. Phys. **40**, 191 (1991).
- [4] J. Villain, J. Phys. C **6**, L97 (1973)
- [5] P.-A. Lindgård and A. Kowalska, J. Phys. **C9**, 2081 (1976)
- [6] M. Steiner and H. Dachs, Solid State Commun. **14**, 841 (1974).
- [7] M. Steiner and J. K. Kjems, J. Phys. **C10**, 2665 (1977).
- [8] B. D. Gaulin, T. E. Mason, M. F. Collins, and J. Z. Larese, Phys. Rev. Lett. **62**, 1380 (1989)
- [9] H. Kadowaki, K. Ubukoshi, and K. Hirakawa, J. Phys. Soc. Japan **56**, 751 (1987).
- [10] W. B. Yelon and D. E. Cox, Phys. Rev. **B7**, 2024 (1973).
- [11] C. Pich, Doctoral Thesis, Technische Universität München (1994).
- [12] M. Steiner, Solid St. Commun. **11**, 73 (1972).
- [13] L. Bonsal and A. A. Maradudin, Phys. Rev. B **15**, 1959 (1977).
- [14] J. M. Ziman, *Principles of the theory of Solids*, (Cambridge Press, 1969), p. 317ff
- [15] S. W. Lovesey, *Theory of Neutron Scattering from Condensed Matter*, Vols. I and II (Oxford, Clarendon) 1984.
- [16] C. Pich and F. Schwabl, Phys. Rev. B **47**, 7957 (1993).
- [17] The lower bound for the exchange energy results from the instability of the spectrum at wave vector  $\mathbf{q}_0$ . A detailed investigation which will be published in a subsequent paper [18], shows that the system will pass through an incommensurate phase at slightly greater

values for  $J'$ . This does not affect the results of this paper.

- [18] C. Pich, F. Schwabl, in preperation
- [19] J. V. Lebesque and N. F. Huyboom, Commun. Phys **1**, 33 (1976).
- [20] M. Steiner and B. Dorner, Solid State Comun. **12**, 537 (1973).
- [21] N. W. Ashcroft and N. D. Mermin, Solid State Physics, Philadelphia.
- [22] J. Jensen and A. R. Macintosh, *Rare Earth Magnetism, Structures and Excitations* (Oxford Science Publications), p. 231ff.

## FIGURES

FIG. 1. The three different magnetic domain types in  $\text{CsNiF}_3$ .

FIG. 2. The crystallographic (—) and magnetic (----) Brillouin zones of  $\text{CsNiF}_3$  in the  $(a^*, b^*)$ -plane. The solid circles ( $\bullet$ ) indicate positions of nuclear Bragg reflections while the open circles ( $\circ$ ) mark the positions of the magnetic Bragg reflections.

FIG. 3. Measured data and fit at  $Q = (0.8, 0, 0)$ ; (----) magnetic excitation and incoherent background; (—) sum signal plus background.

FIG. 4. Field dependence of signal at  $Q = (0.7, 0, 0)$ . The solid lines are guides to the eye. The Insert shows field dependent intensity of the magnetic reflection at  $(0.5, 0, 0)$ .

FIG. 5. Measured data and fit at  $Q = (0.8, 0, 2)$ ; (----) magnetic excitation of domains (B),(C) with fixed energy determined by the measurements at  $(0.8, 0, 0)$ ; (.....) magnetic excitation of domain (A) and incoherent background; (—) sum signal plus background.

FIG. 6. The dispersion relation fitted to the measured data. The numbers at the lower abscissa denotes the  $\mathbf{q}$ -position along the  $a^*$  and  $b^*$  axes in the first Brillouin zone. The letters at the upper abscissa correspond to special points in the Brillouin zone (Fig. (2)). The in-plane mode  $E_q^{(1)}$  and out-of-plane mode  $E_q^{(2)}$  are shown by the solid and dashed lines, respectively. A striking feature is the jump of the in-plane mode at  $\Gamma$ .

FIG. 7. Schematical representation of the spin wave induced dynamical in-plane magnetization ( $\Rightarrow$ ) for long wavelengths. Two cases are shown: wave vector  $\mathbf{k}$  parallel (a) and perpendicular (b) to the ordered moments. The dipole energy differs between both cases, leading to the jump of the dispersion relation at  $\Gamma$ .

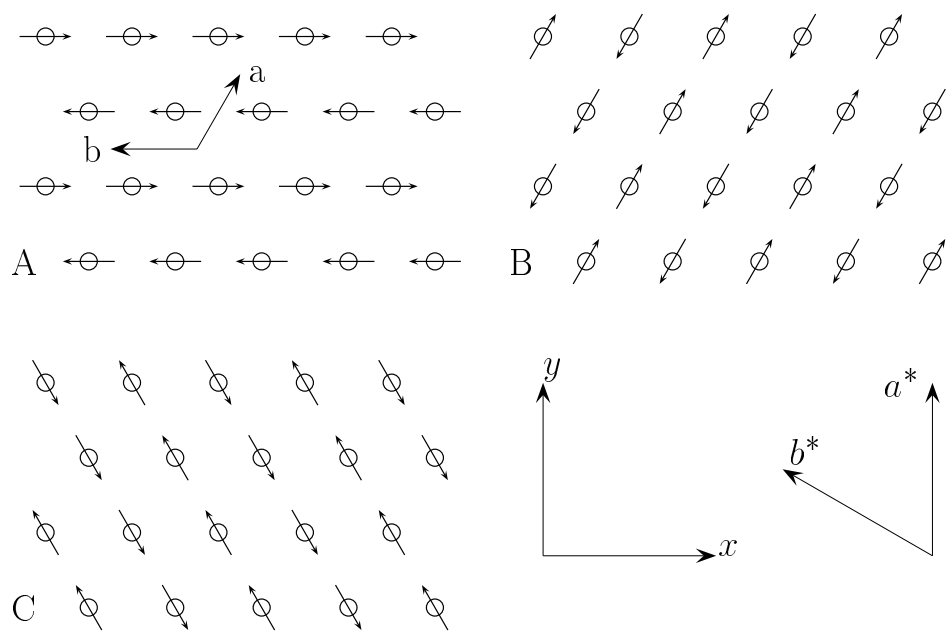


Fig. 1

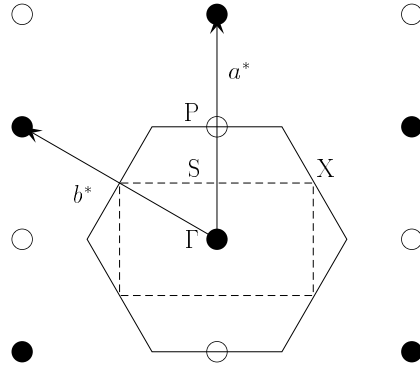


Fig. 2

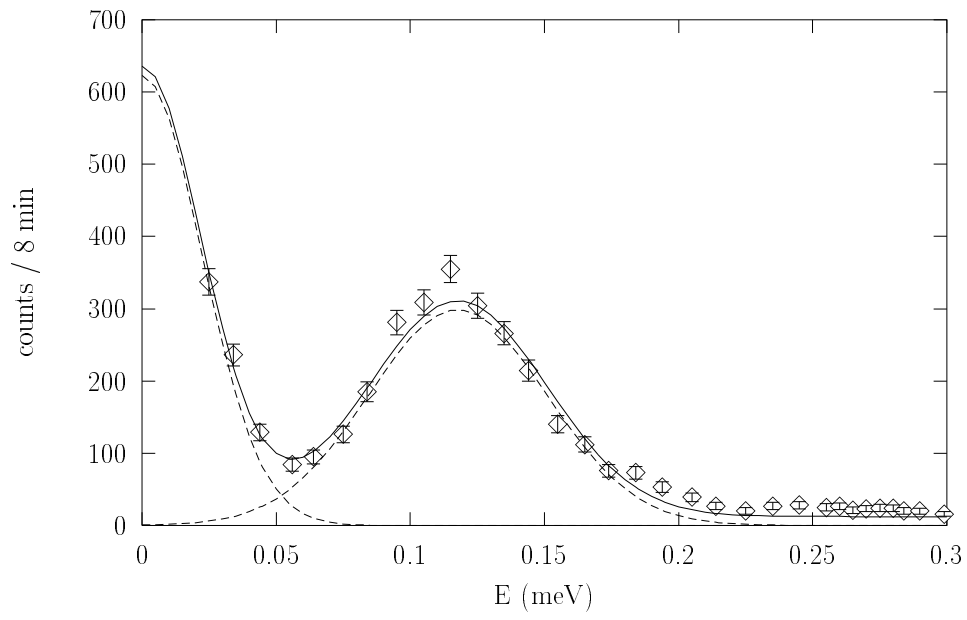


Fig. 3



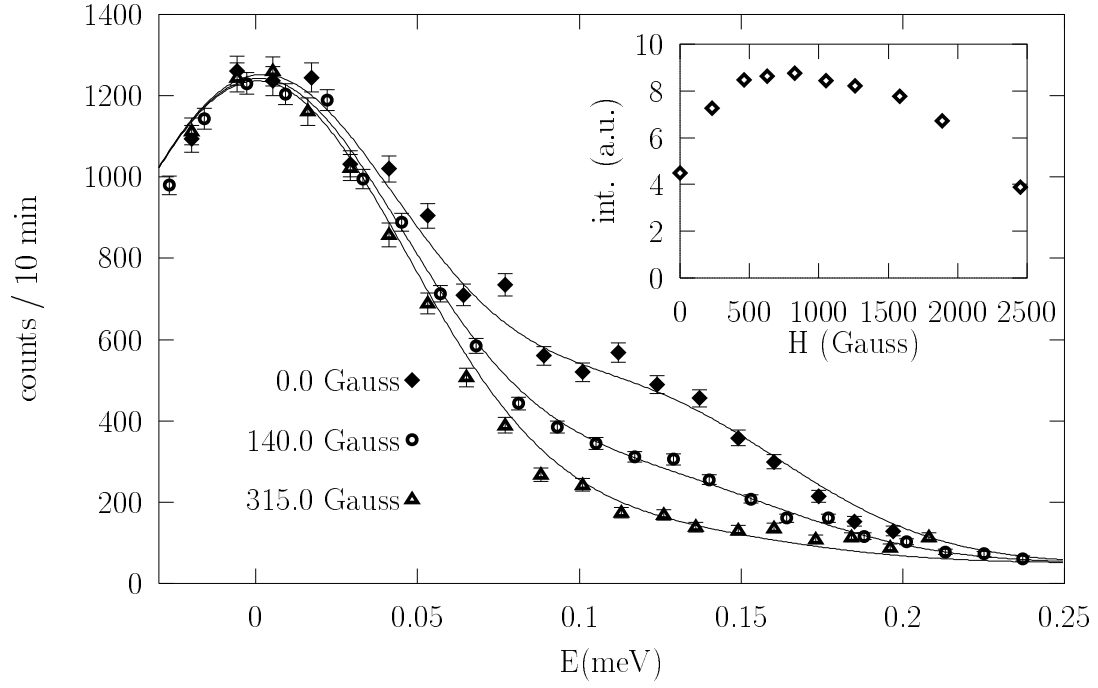


Fig. 4

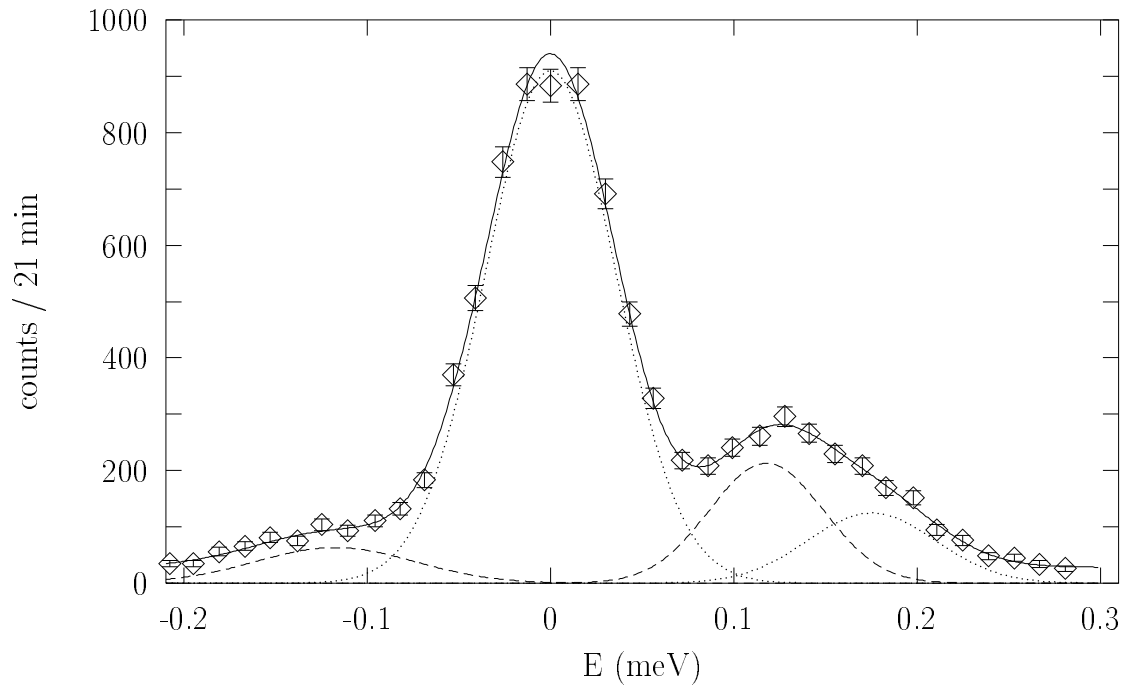


Fig. 5

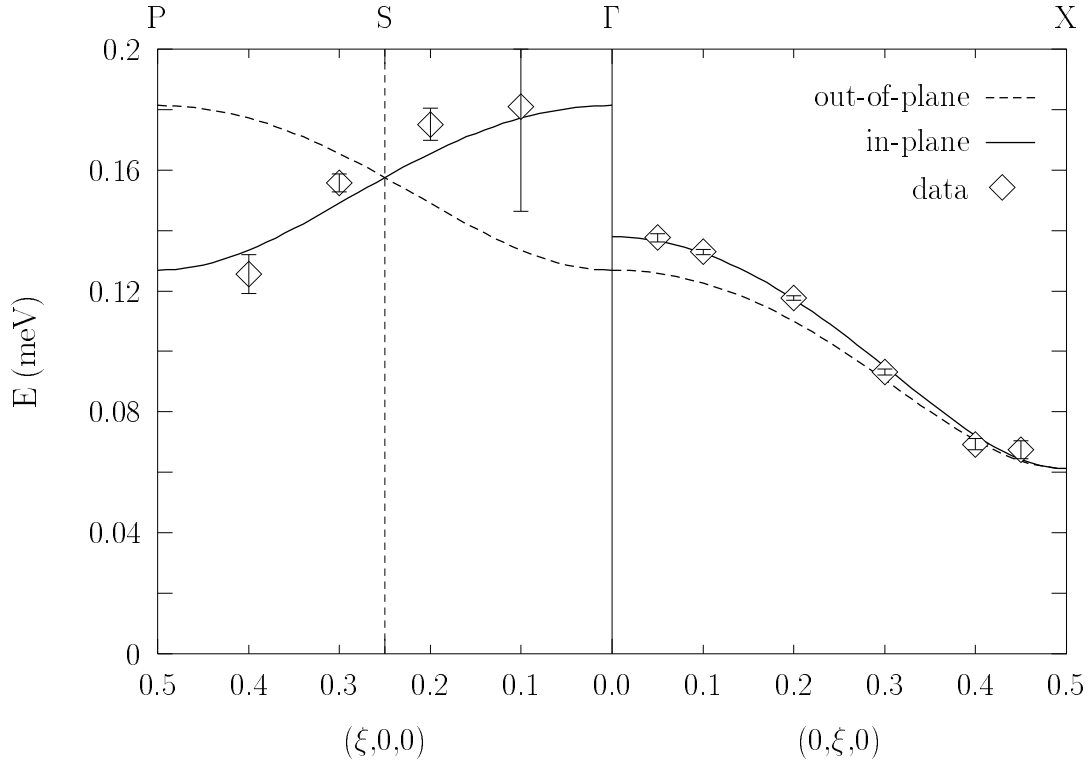


Fig. 6

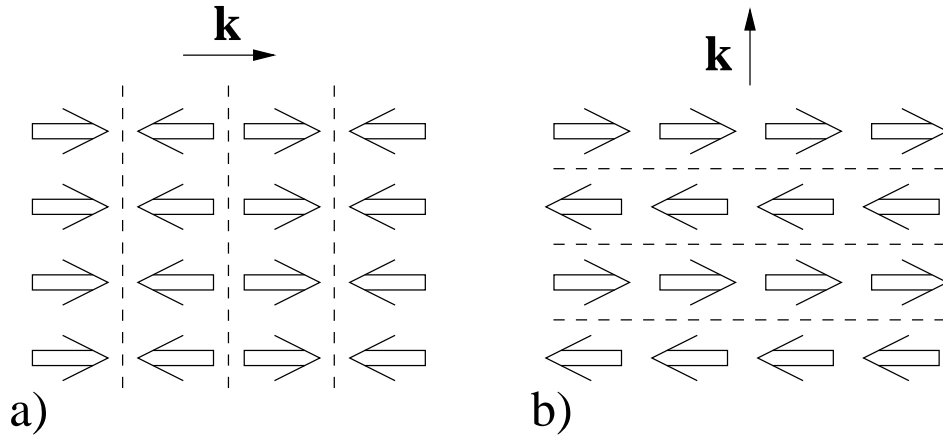


Fig. 7